Chiral Symmetry Breaking in Liquids and Critical Point Confluence

The geometry of molecules residing in solid, liquid, and vapor phases is obviously a basic issue in chemistry, chemical physics, materials science, and molecular biology. In particular, the chirality (handedness) of molecules frequently demands attention. Polymeric biological molecules (proteins, DNA, carbohydrates, ...) contain subunits that typically exhibit a specific chiral geometry choice, avoiding its mirror image. What caused this broken geometric symmetry to arise and to influence first appearance of life and its subsequent evolution on our planet? Was this terrestrial chiral bias an absolute necessity for life as we define it? If so, how far must one search in the universe to discover other H,C,N,O,P based life with chirality opposite to our own? This lecture concentrates on one among many possibilities of spontaneous chiral symmetry breaking phenomena, among which geochemists must decide was most likely involved in our prebiotic history.

View 1. Title, Lecturer, Affiliation, Acknowledgements, Widom Festschrift reference.

To serve as a familiar starting point, View 2 illustrates the two enantiomers

---

View 2. Alanine enantiomers.

(mirror images) of the simple protein-monomer amino acid alanine in isolation, identifying which one is biologically favored. In this case it is the strong tetrahedral directionality of four covalent single bonds emanating from the "α-carbon" ("stereo carbon") that produces a pair of mirror-image twins. These distinct alanine molecules are separated by a high transition state barrier of approximately $78 kcal/mol$, much larger than ambient kinetic energy $k_B T \approx 0.6 kcal/mol$. However there are many other molecular scenarios that also generate distinguishable chiral enantiomers, not necessarily relying on the presence of tetrahedral stereocarbons. The following View 3 provides the contrasting

---

View 3. Hydrogen peroxide enantiomers.

---

example of the isolated hydrogen peroxide molecule. Quantum mechanical calculations indicate that for this case the inversion barrier located at a planar transition state (*trans* geometry) is only approximately $1.1 kcal / mol$.

The main emphasis of this presentation concerns spontaneous chiral symmetry breaking in pure isotropic liquids. Here attention focuses on an initially racemic isotropic liquid at elevated temperature composed of molecules that have high inversion rates. Lowering the temperature ultimately produces macroscopic isotropic liquid phases within each one of which one chirality strongly dominates. This is a phenomenon that now has unequivocal experimental support. View 4

View 4. 138-atom molecular structure. [Coexisting chiral liquids exist thermodynamically between a lower temperature bicontinuous cubic phase, and a higher temperature single isotropic achiral liquid phase.]

---

presents the molecular structure of a flexible 138-atom organic substance that has been shown to exhibit isotropic chiral liquid phases at 1 atm in the temperature range $205^{\circ}C - 213^{\circ}C$. The chiral nature of the liquids is demonstrated by observing them with a polarimeter. View 5 reproduces the published patterns seen

---

View 5. Polarimetry results.

---

by a microscope view of a thin film sample in the mentioned temperature range. Coexisting immiscible liquid phases of this pure substance are then distinguished by changing the angle between incident light polarity and the polarimeter detector (analyzer). Isotropy of the phases is demonstrated by noting that no intensity pattern changes as the sample is rotated while the polarity-analyzer relative angle remains constant. At P-A angle 90° the phases would be visibly indistinguishable.

Positive surface tension interfaces are clearly visible in the polarimetry observations. Because their presence amounts to a positive free energy source, a statistical driving force exists for one of the chiral liquids ultimately to consume the other. However that evidently is a very slow process for this substance.

The specific 138-atom substance is not unique in exhibiting the formation of immiscible pairs of isotropic chiral liquid phases. The next View 6 identifies a

---

View 6. Additional substances producing isotropic chiral liquids.

---

published listing of several other experimentally identified cases. In all of these substances no tetrahedral-bonding stereocarbons appear, but the individual molecules are quite flexible objects. If one were able to examine exhaustively the

intramolecular force field for one such molecule in isolation (*i.e.*, *in vacuo*), one would surely discover numerous mechanically stable distorted structures, including mirror image chiral pairs. In a cooling liquid state, intermolecular interactions can have the effect of probabilistically selecting neighbor pairs with favorable relative configurations. For these various experimentally observed cases this has led to spontaneous appearance of preferential chirality in isotropic liquid phases.

The organic molecules just identified have a large number of internal degrees of freedom, a situation that can be distracting in an attempt to understand quantitatively what underlies the phenomenon of spontaneous chiral symmetry breaking in pure isotropic liquids. Consequently it has been sensible to create a simpler theoretical model exhibiting this phenomenon prior to undertaking a massively complex explanation of the experimentally studied cases. The following View 7 introduces an elementary continuum model that my collaborators and I

View 7. Tetramer enantiomers, stable structures. [F. Latinwo, F.H. Stillinger, and P.G. Debenedetti, J. Chem. Phys. **145**, 154503 (2016)]

---

have examined recently. In a rough sense it was inspired by the four-atom hydrogen peroxide example. For each of its two mechanically stable structures (intramolecular potential energy global minima), it possesses three equal "covalent" bond lengths b, two intramolecular 90° bond angles at each of the two internal "atoms" , and a $\pm 90^\circ$ dihedral angle, the sign of which distinguishes the two enantiomers.

A basic property of this continuum model is how the molecule's potential energy rises as deformations away from the global minima are imposed. View 8

View 8. Tetramer intramolecular deformation energy expression, shown with dimensionless parameters.

---

provides full details. This involves harmonic contributions for bond-length change, and for bond angle change. The square of the cosine of the dihedral angle controls the transition state energies (at either *cis* or *trans* planar geometries) which must be surmounted for chiral inversion.

In order to have a mathematically unambiguous identification scheme for the two tetramer enantiomers, even when they might be subject to arbitrary large intramolecular deformations, it is natural to classify the tetramers according to their values of a geometric quantity ζ defined in View 9. This is a function of

---

View 9. Definition of $\zeta(1,2,3,4)$. [Can be used to determine sign of φ]

---

the three intramolecular vector bond displacements, and as defined is confined to the interval $-1 \le \zeta \le +1$. The upper and lower limit values are attained respectively by the two undeformed mechanically stable configurations. It is simply the algebraic sign of ζ that is the enantiomer identifier. Planar configurations have $\zeta = 0$, which identifies the hypersurface separating the two configurational manifolds for the mirror-image enantiomers.

In order for this simple tetramer model to mimic the ability of the previously mentioned complicated molecules to produce isotropic immiscible chiral liquids, it is necessary to define appropriate pair intermolecular interactions. This has been done in a way that incorporates both indiscriminately attractive interactions, as well as chirality-dependent interactions. The following View 10 indicates how this

---

View 10. Chirality-sensitive tetramer pair interaction.

---

is implemented, starting with the well-known Lennard-Jones 12-6 pair potential acting between an "atom" (force center) in one of the tetramers and an "atom" (force center) in the other tetramer. However the resulting sum of 16 Lennard-Jones interactions is energy-strength-scaled in a way that depends specifically on the instantaneous ζ values for the two tetramers. This effect is controlled by the scalar parameter $-1 < \lambda < +1$. Because this mathematically converts each of the Lennard-Jones pair functions into "eight-atom" functions, it can be regarded as a coarse-grained chirality preference interaction strategy for neighboring tetramers.

The continuum tetramer model has been examined via a modest amount of molecular dynamics simulation. The majority of computations completed thus far have employed a dimensionless set of interaction parameters, as listed in View 11.

View 11. Dimensionless parameters for tetramer model simulations.

For these and some other selections of potential energy parameters with various physical conditions the model indeed exhibits spontaneous formation of immiscible isotropic chiral liquids upon cooling a racemic state. View 12 shows -

---

View 12. Molecular dynamics result for low-T growth of $\langle \zeta \rangle$ away from 0; $\lambda = 0.5$; opposite enantiomers are distinguished by red *vs*. blue coloring.

[State reference. $N = 1024,\ \rho\sigma^3 = 0.17,\ k_B T / \varepsilon_0 = 1.4$]

[A higher temperature MD run with an enantiopure initial condition would qualitatively reverse the time dependence, ending up racemic.]

---

an example of a time sequence for $\lambda = 0.5$ over which an initial racemic mixture evolves into a contacting pair of chiral liquids with opposite $\langle \zeta \rangle$ values. This phase separation kinetically involves both tetramer inversion and diffusion. Upon carrying out these simulations at several temperatures for the same number density, one infers that the temperature variation of $\langle \zeta \rangle$ exhibits a "conventional" critical point behavior as qualitatively indicated in the next View 13. For the previously

---

View 13. Isochoric plot of $\langle \zeta \rangle$ *vs.* T.

---

illustrated density $\rho\sigma^3 = 0.17$ and $\lambda = 0.5$, the estimated critical temperature is $k_B T_c / \varepsilon_0 \approx 2.3$. The isochoric plot indicates that the chiral liquids would finally crystallize as temperature falls, however that phase transition for the continuum tetramer model has only been incompletely examined thus far. [Tentative result: triclinic, 2 tetramers per unit cell]

The tetramer model includes Lennard-Jones attractive interactions between neighboring molecules of some magnitude regardless of whether their respective chiralities are relatively favored or disfavored by the λ choice. Consequently it is reasonable to expect that in principle the tetramer model might also exhibit a second critical point, specifically a conventional liquid-vapor critical point, among its set of thermodynamic equilibrium states. It is worth noting in passing that a pair of critical points are also observed in real fluid systems at thermal equilibrium, namely upper and lower consolute critical points, examples of which are referenced in View 14. However this latter phenomenon does not involve

---

View 14. Experimentally observed cases of critical point pairs at equilibrium.
Nicotine-water.

---

spontaneous appearance of chirality, and so is only indirectly related to the possible scenario presented by the continuum tetramer model. [Perhaps it might be worth mentioning the distinction between these thermal equilibrium cases of pairs of critical points, and the case of water with its second critical point located within the metastability domain.]

Because computer simulation has not yet undertaken the necessarily demanding search for conventional liquid-vapor critical points that might be generated in the continuum tetramer model, there is virtue in temporarily creating and analyzing an even more elementary lattice model that could simultaneously present both chiral-symmetry-breaking, and liquid-vapor, critical points. The properties of this

elementary model could ultimately assist in extended study of the tetramer model. Such an elementary lattice model should be constructed to mimic roughly the qualitative characteristics of the continuum tetramer model. Details of such a discrete description appear in View 15. Specifically this amounts to a spin-1 Ising

---

View 15. Lattice model basic definition: spin-1 Ising model with spatially extended pair interactions, ν_i , N_+, N_- ; spin inversion symmetry.

---

model with possibly spatially extended pair interactions. It is based upon a three-dimensional Bravais lattice (*e.g.*, a simple cubic lattice) of M cells, each one of which can contain at most a single chiral molecule. The cells are identified by index $1 \le i \le M$, with corresponding occupancies which are specified by "spin" variables $\nu_i = -1, 0, +1$; these represent respectively a left handed molecule L, no occupying molecule, and a right handed molecule D.

View 16. Cartoon image of occupied lattice.

The following View 17 involves the interaction potential Φ for this spin-1

View 17. $\Phi(\nu_1 ... \nu_M)$ in terms of $\varphi_J(r_{ij})$ and $\varphi_K(r_{ij})$; canonical partition function.

---

system, which must be invariant to overall spin inversion. By analogy with the continuum tetramer model, it is assumed that only pairs of spins contribute to Φ , with magnitudes depending on the scalar distance between the respective occupied cells, and on the relative chirality of the occupants. This View 17 also displays the classical canonical partition function for the lattice model.

It is well known that exact evaluations in the large system limit are not available for three-dimensional Ising models, even for the cases of spin-1/2 with just nearest-neighbor interactions. But to infer statistical properties in at least a semi-quantitative manner, one can traditionally invoke the so-called "mean field approximation". This tactic is outlined in View 18, where it is applied to the

---

View 18. Mean field approximation; $J, K < 0$.

---

canonical partition function for the spin-1 model. The principal tactic underlying the mean field approximation is to suppose that the neighborhood of any molecule-inhabited cell is composed of particle concentrations equal to the overall average for the entire lattice. This has the effect of replacing the local φ_J and φ_K sums in

Φ respectively by constants *J* and *K*. Both of these constants will be assumed to be negative (a) to conform to normal molecular dispersion attraction, and (b) to be relevant to the present focus on chiral symmetry breaking. For any specific molecular pattern on the lattice of cells, intensive quantity $-1 \le x \le +1$ describes the net chiral bias.

The relative values of interaction parameters *J* and *K* control the appearances of the two possible equilibrium critical points. If one initially wishes to have a chirality preference appear first as temperature is lowered from a high value isochorically, one should set $|K| >> |J|$. View 19 then shows how the mean-field

---

View 19. Chiral symmetry breaking for $|J| << |K|$; nonlinear equation for $x(T)$.

---

partition function predicts the existence of chiral symmetry breaking by generating a nonlinear equation for $x(T)$.

Numerical solution of that nonlinear equation leads to the plot displayed in the next View 20, showing $x(T)$ splitting continuously from the high-*T* racemic

---

View 20. Plot of $x(T)$; $k_B T_{\pm} = -K\rho$; no crystal structure predicted.

---

value 0 to a symmetric pair of non-zero values representing mirror-image phases. This critical point description conforms to the conventional mean-field result of a square-root (inverted parabola) shape of the coexistence region as a function of temperature. Note that the critical point temperature $T_{\pm}$ is predicted to be proportional to the molecular number density $\rho = N / M$.

Next, consider the reversed case $|J| >> |K|$, which should generate a liquid-vapor critical point for the racemic fluid at a temperature well above any chiral symmetry breaking propensity. Locating the occurrence of the liquid-vapor critical point at $x = 0$ and related spinodal curves requires identifying divergence of the isothermal compressibility as a function of *T* and ρ. This can be accomplished using the pressure equation of state for the homogeneous racemic fluid, in the mean-field approximation for the lattice model. View 21 displays that pressure

---

View 21. Liquid-vapor critical point identification considerations for $|J| >> |K|$. Lattice model mean-field approximation for $p\omega$.

---

function.

Specifically, the critical point and the associated spinodal curves are located by the vanishing of the isothermal derivative $\left(\frac{\partial p\omega}{\partial(1/\rho)}\right)_T$, the specific form of which appears in the following View 22. In order to identify the coexisting liquid and

---

View 22. Critical point and spinodal curves from $[\partial p\omega/\partial(1/\rho)]_T = 0$; real solutions formula; $k_B T_{lv} = -J/4$, $\rho_{lv} = 1/2$. Maxwell construction for coexisting densities below T_{lv}.

---

vapor densities when $T < T_{lv}$, it is necessary to invoke the Maxwell equal-areas construction to assure that the chemical potentials for those coexisting fluids are equal. The resulting densities to leading order in temperature reduction are specified in this View 22.

Under the isochoric condition $\rho = 1/2$, and with the two negative coupling constants satisfying $|J| > 2|K|$, both types of critical points will be observed, with $T_{lv} > T_{\pm}$. The following View 23 provides a schematic diagram of how the

---

View 23. Schematic plot in x, ρ, T space of homogeneous phases with $T_{lv} > T_{\pm}$; three distinct surface tension functions.

---

individual homogeneous phases that would coexist under the isochoric condition would be located in x, ρ, T space. It is a significant fact that three distinct interfacial surfaces will appear under the imposed isochoric condition, each with its own temperature-dependent surface tension. These are (a) the interface between the racemic liquid and vapor for $T_{lv} \geq T \geq T_{\pm}$, (b) the interface between the pair of chiral liquids for $T_{\pm} \geq T$, and (c) the interface between a chiral liquid and the racemic vapor for $T_{\pm} \geq T$.

The obvious next issue is what happens at $\rho = 1/2$ if the temperature difference between the two critical points vanishes: $T_{lv} = T_{\pm}$. In other words, what interaction choices cause confluence of the two critical points. View 24 contains

---

View 24. Critical point confluence conditions: $\rho_{cfl} = 1/2, J = 2K$; $k_B T_{cfl} = |J|/4 = |K|/2$.

---

relevant details of this special circumstance.

View 25 shows a schematic plot of the homogeneous-phase intensive properties

---

View 25. Schematic plot in x, ρ, T space of homogeneous phases for $T_{lv} = T_{\pm} = T_{cfl}$; two distinct surface tension functions.

---

in the three-dimensional x, ρ, T space for the confluence case. Note that in this situation there are only two observable interfaces with respective surface tensions: (a) the interface between the two immiscible isotropic chiral liquids, and (b) the interface between a chiral liquid and the racemic vapor. These both arise for $T_{cfl} \geq T$.

Confluence of the two critical points produces at least one additional unusual detail, the basic features of which are outlined in View 26. A qualitatively

---

View 26. Mean field approximation prediction of modified critical exponent for chiral symmetry breaking magnitude *vs.* $\Delta T = T_{cfl} - T$. $\Delta\rho = \rho - 1/2$.

$$x \propto \pm(\Delta\rho)^{1/2}$$

$$\propto \pm(|\Delta T|^{1/2})^{1/2}$$

$$= \pm|\Delta T|^{1/4} \quad .$$

---

distinct outcome emerges from the critical behavior of the extent of chiral symmetry breaking. This arises in connection with the density variation of $T_{\pm}$ indicated earlier. As a result of the confluence, the chiral symmetry breaking phenomenon is not subject to a fixed number density ρ , but to the liquid density rising by an amount proportional to $|\Delta T|^{1/2}$ as *T* declines. Consequently the applicable symmetry-breaking parameter *x* exhibits the leading-order temperature dependence specified in View 26. Thus the critical exponent controlling the rate of chirality bias as *T* declines has been cut in half.

Having discussed the effects at the half-filled density $\rho = 1/2$ of raising the chiral-symmetry-breaking critical point temperature $T_{\pm}$ from substantially below T_{lv} until these two coincide, it is natural to inquire whether continuation of this relative temperature trend at the same overall system density 1/2 can yield a non-trivial situation where again two critical points appear with $T_{\pm} > T_{lv}$. A straightforward analysis indicates that upon isochoric cooling, an initially appearing high-temperature chiral liquid at this density 1/2 would not exhibit a liquid-vapor critical point. Instead, cooling the chiral liquid phase would cause its pressure to decline until it equaled an equilibrium

racemic-vapor pressure, at which point a first-order vaporization transition would occur. In other words, when $|2K| > |J|$, the high temperature chirality occurrence pre-empts subsequent appearance upon further cooling of a conventional liquid-vapor critical point, at least as predicted within the mean field approximation.

A final View 27 lists a few directions along which the subject discussed could

---

View 27. Opportunities for future research, experimental and theoretical. [renormalization group approach; synthesize more molecules exhibiting these phenomena; Monte Carlo simulations for lattice model (study effects of interaction range, etc.); measure the interfacial surface tensions and determine their critical exponents; achiral solvents; patchy colloids; MD search for critical points in tetramer continuum model].

---

be expanded and strengthened scientifically.

Spontaneous Chiral Symmetry Breaking in Liquids

Frank H. Stillinger
Department of Chemistry, Princeton University

Acknowledgement:

Insightful discussions with Prof. Pablo G. Debenedetti, Department of Chemical and Biological Engineering, Princeton University

Published reference:

Benjamin Widom 90th Birthday Festschrift issue, J. Phys. Chem. B **122** (13), 3441-3446 (2018)

View 2 (click to go back)

AMINO ACID EXAMPLE: ALANINE

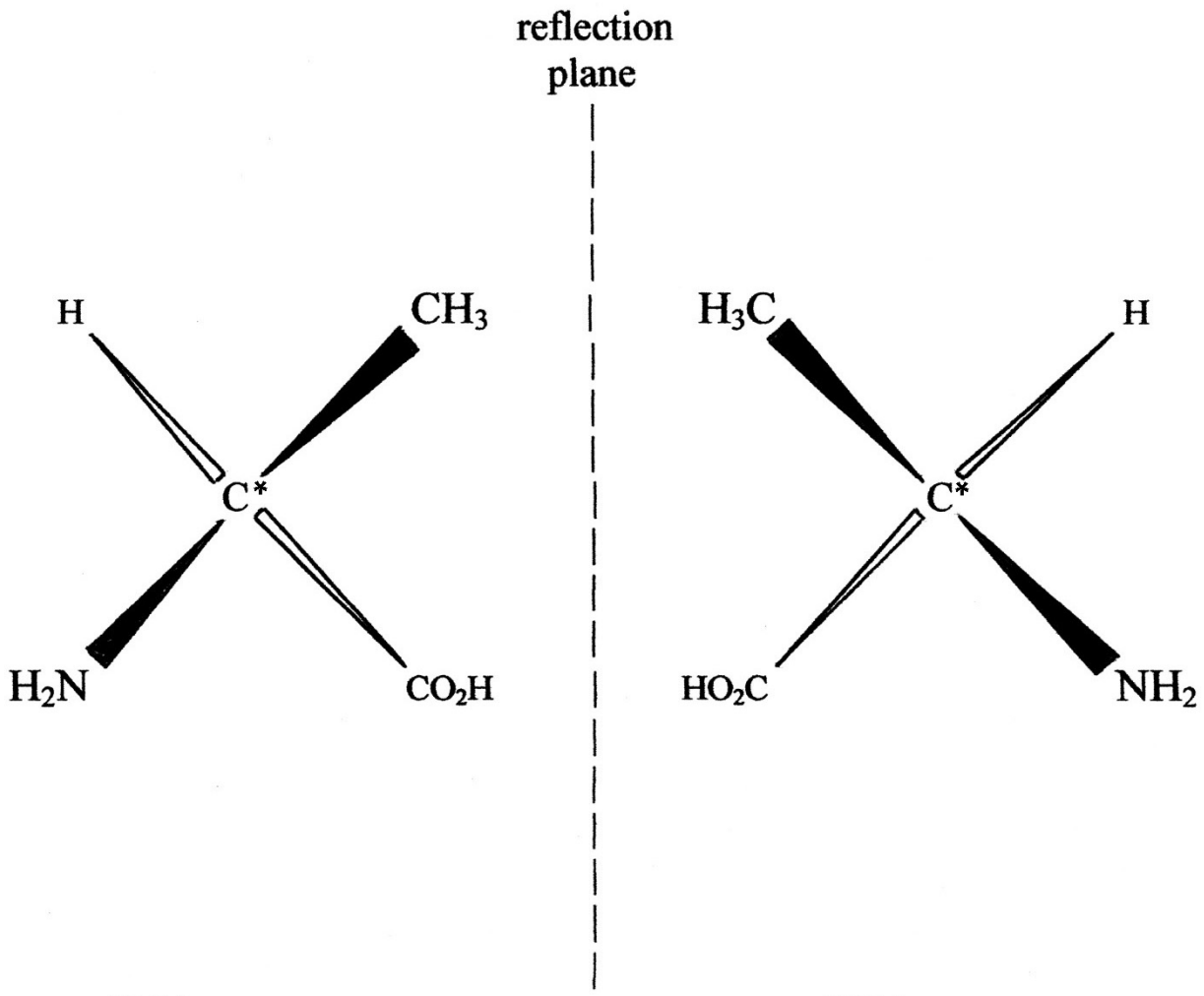

"L" isomer

biologically favored

"D" isomer

Hydrogen Peroxide Stable Structures

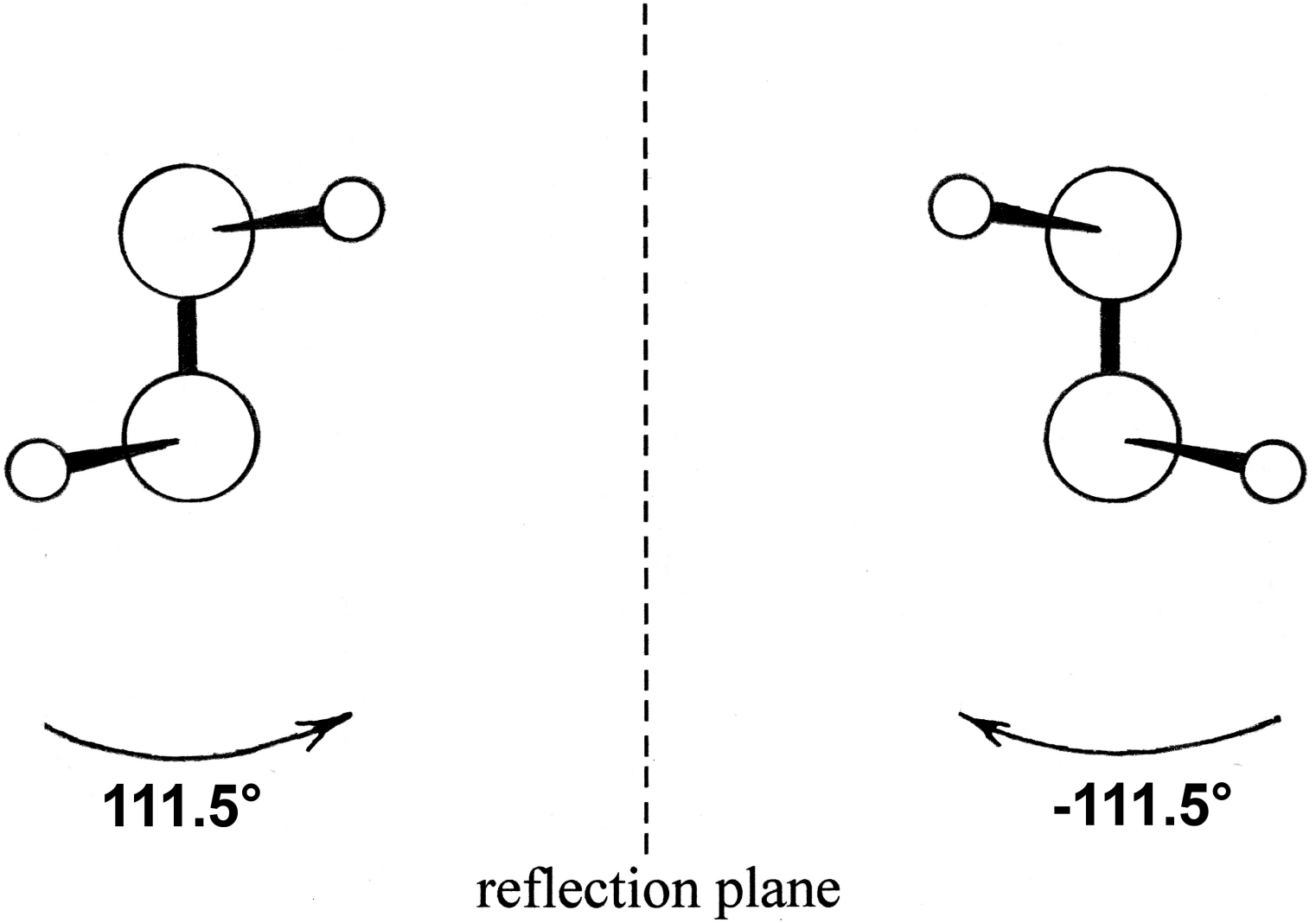

Immiscible Pairs of Isotropic Chiral Liquids

Reference:

C. Dressel, T. Reppe, M. Prehm, M. Brautzsch, and C. Tschierske, *Nature Chemistry* **6**, 971-977 (2014), "Chiral self-sorting and amplification in isotropic liquids of achiral molecules".

Molecular structure (R = *n* - C_6H_{13}):

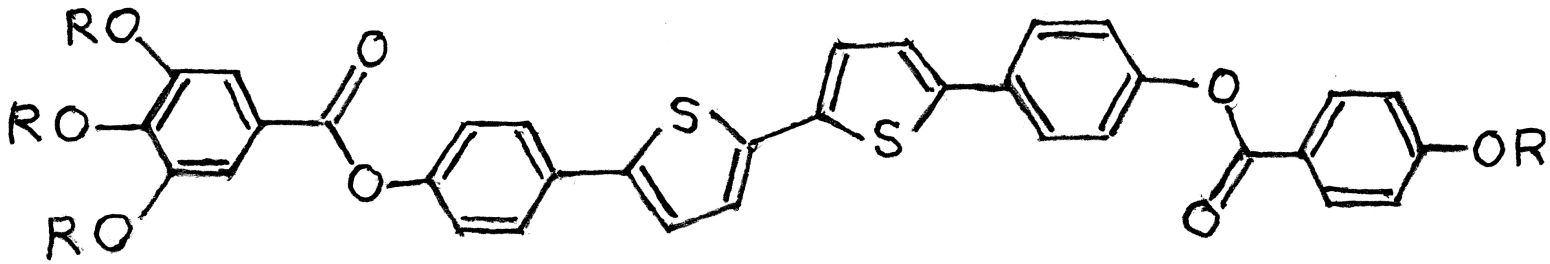

Approximate temperature range of immiscibility: $205^{\circ}\mathrm{C} \leq T \leq 213^{\circ}\mathrm{C}$

View 5 (click to go back)

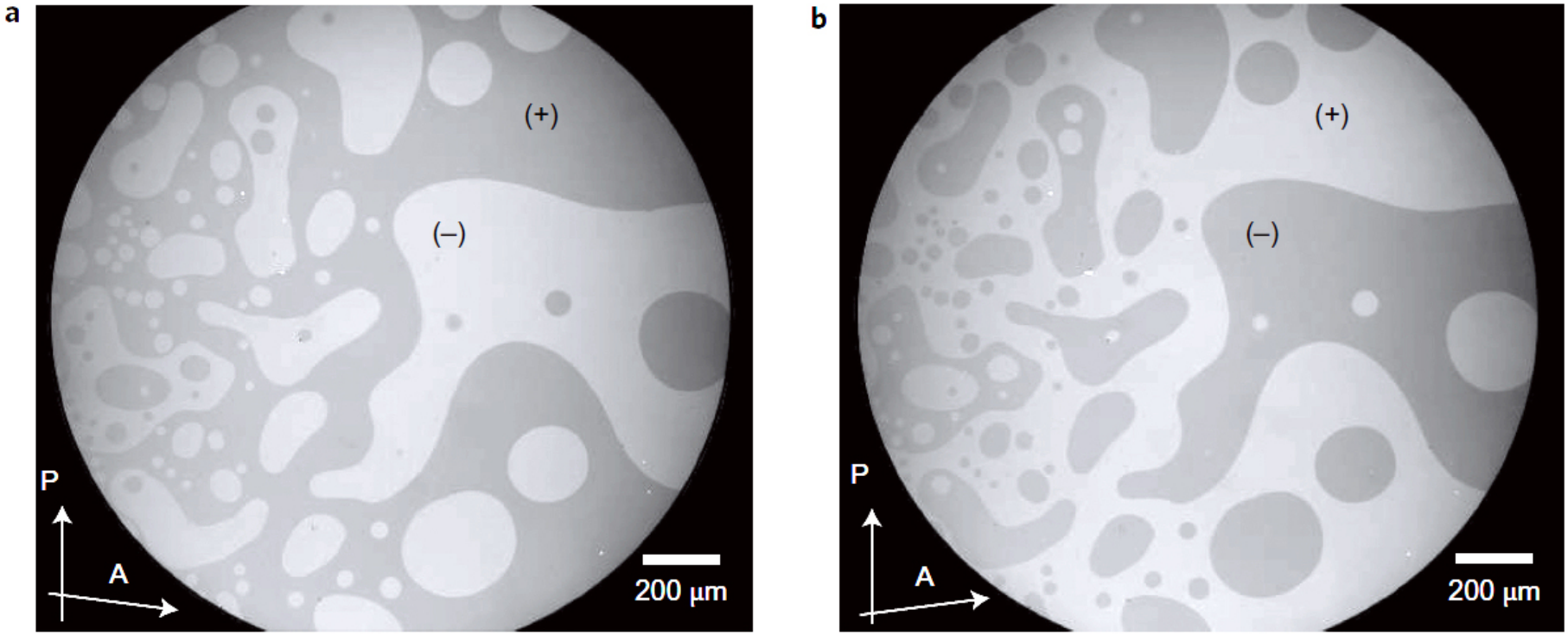

Additional Molecular Substances Experimentally Exhibiting Isotropic Chiral Liquids

- Relevant reference:
  C. Tschierske and G. Ungar, *ChemPhysChem* **17**, 9-26 (2016), "Mirror Symmetry Breaking by Chirality Synchronisation in Liquids and Liquid Crystals of Achiral Molecules"

- Eight distinct organic examples cited in Scheme 3 and Table 1.

- None of the molecular structures of these additional substances contains stereocarbons.

Flexible Tetramer Model, Stable Structures

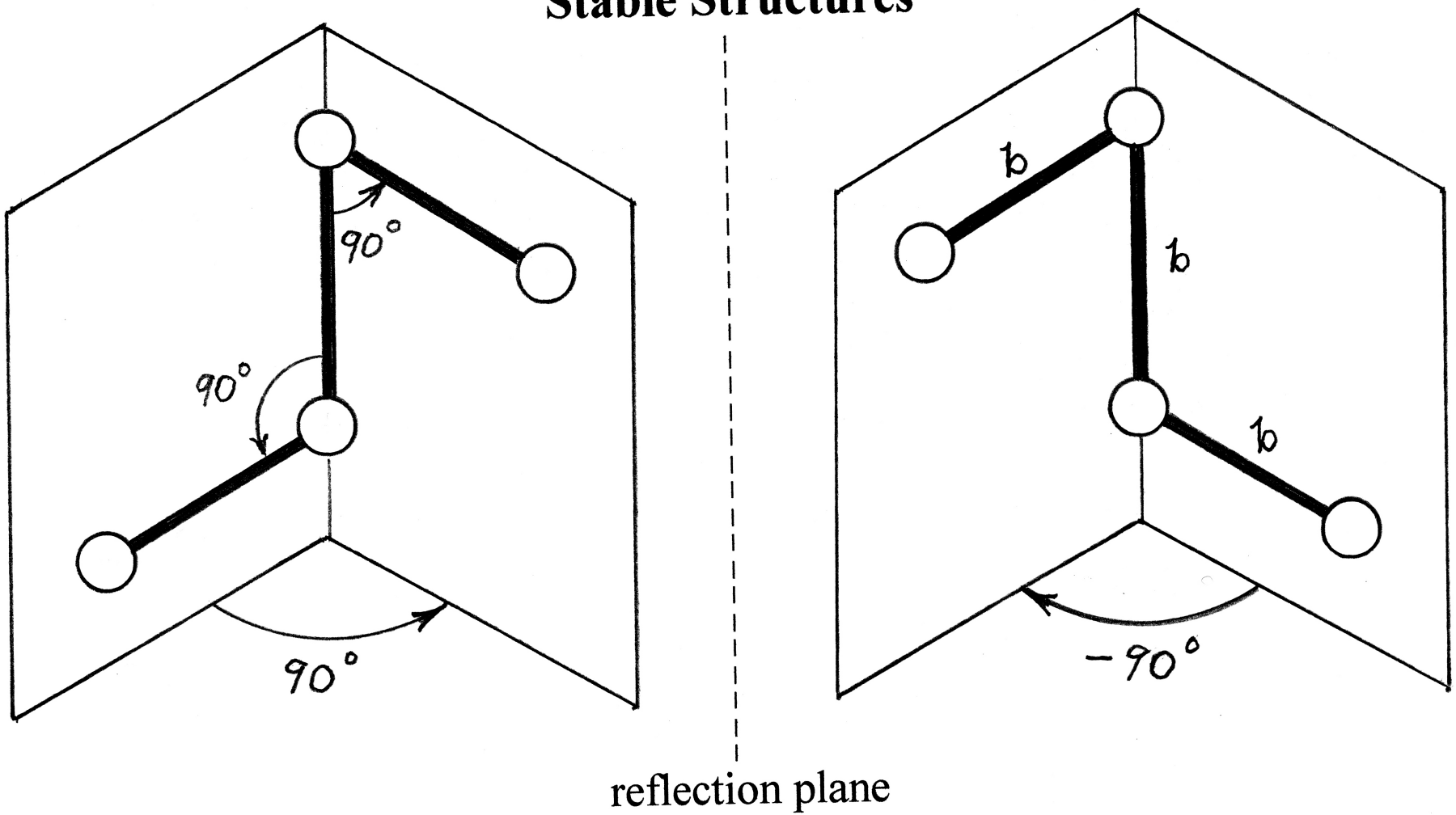

Tetramer Intramolecular Potential Energy

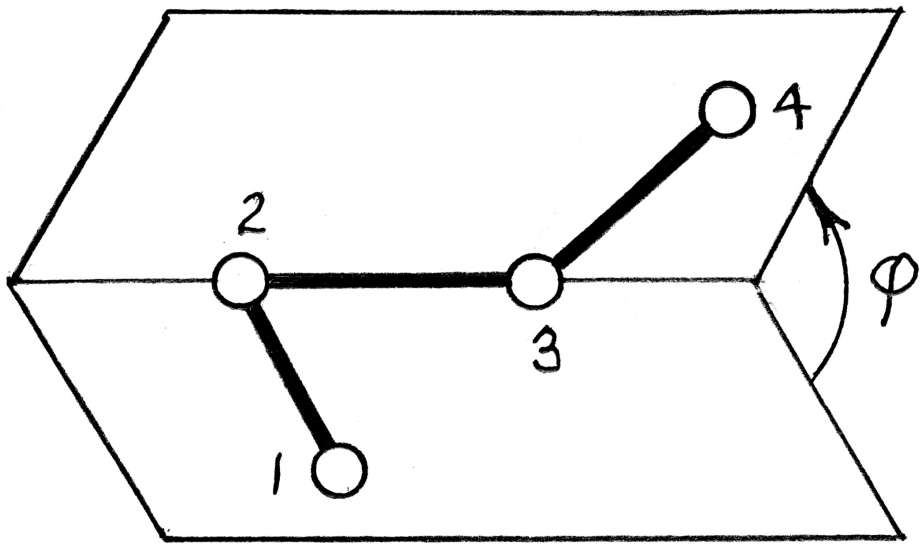

$$\Phi^{(1)}(\mathbf{r}_1,\mathbf{r}_2,\mathbf{r}_3,\mathbf{r}_4) = \sum_{i=1}^{3}(K_{str}/2)(r_{i,i+1}-b)^2 + \sum_{i=2}^{3}(K_{bnd}/2)(\theta_i-\pi/2)^2 + K_{dih}\cos^2\varphi \quad .$$

Dihedral angle $-\pi \le \varphi \le \pi$ definition:

$$\cos\varphi = \frac{(\mathbf{r}_{12}\times\mathbf{r}_{23})\cdot(\mathbf{r}_{23}\times\mathbf{r}_{34})}{|\mathbf{r}_{12}\times\mathbf{r}_{23}||\mathbf{r}_{23}\times\mathbf{r}_{34}|} \quad .$$

Chirality Measure for Individual Tetramers

- Monomers located at $\mathbf{r}_1, \mathbf{r}_2, \mathbf{r}_3, \mathbf{r}_4$.
- $\zeta(\mathbf{r}_1,\mathbf{r}_2,\mathbf{r}_3,\mathbf{r}_4) = \dfrac{\mathbf{r}_{12}\cdot(\mathbf{r}_{23}\times\mathbf{r}_{34})}{|\mathbf{r}_{12}||\mathbf{r}_{23}||\mathbf{r}_{34}|} \equiv \dfrac{\mathbf{r}_{43}\cdot(\mathbf{r}_{32}\times\mathbf{r}_{21})}{|\mathbf{r}_{43}||\mathbf{r}_{32}||\mathbf{r}_{21}|}$.
- $-1 \le \zeta \le +1$; $\zeta = \pm 1$ at the $\Phi^{(1)}$ minima .
- $\zeta = 0$ for tetramer planar configurations, including the ideal transition states.
- Enantiomeric excess ("ee"): $-1 \le (N_+ - N_-)/(N_+ + N_-) \le +1$

Tetramer Pair Interaction ($\Phi^{(2)}$)

- Sixteen energy-scaled Lennard-Jones pair interactions between monomers belonging to different tetramers (α, γ):

$$\Phi^{(2)} = \sum_{i=1}^{4} \sum_{j=1}^{4} \varepsilon_{mm}(\zeta^{(\alpha)}, \zeta^{(\gamma)}) \mathrm{v}_{\mathrm{LJ}}(|\mathbf{r}_i^{(\alpha)} - \mathbf{r}_j^{(\gamma)}|/\sigma_0) \ .$$

- $\mathrm{v}_{\mathrm{LJ}}(x) = 4(x^{-12} - x^{-6})$.

- $\varepsilon_{mm}(\zeta^{(\alpha)}, \zeta^{(\gamma)}) = \varepsilon_0(1 + \lambda\zeta^{(\alpha)}\zeta^{(\gamma)})$, where $|\lambda| < 1$.

- $\lambda > 0$ favors like enantiomers, $\lambda < 0$ favors opposite enantiomers.

- ε_{mm} varies smoothly as the tetramers deform, passing through ε_0 when one tetramer changes chirality.

Parameter Choice, Reduced Units

- Elementary parameter set choice: m, ε_0, σ_0
- Time unit: $\sigma_0 (m/\varepsilon_0)^{1/2}$
- Number density unit: σ_0^{-3}
- Temperature unit: ε_0 / k_B
- Pressure unit: $\varepsilon_0 / \sigma_0^{3}$
- Dimensionless intramolecular ($\Phi^{(1)}$) parameters:

$K_{str} = 8003, \quad K_{bnd} = 643.7, \quad K_{dih} = 17.86, \quad b = 1.0583$

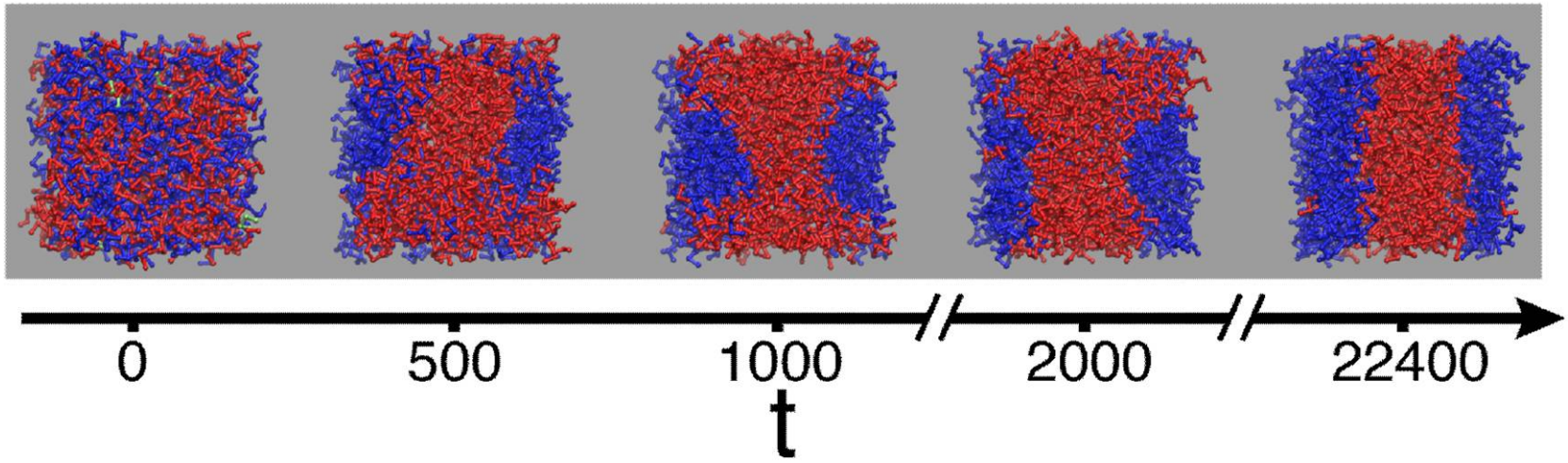

(T=1.4, tetramer number density = 0.17)

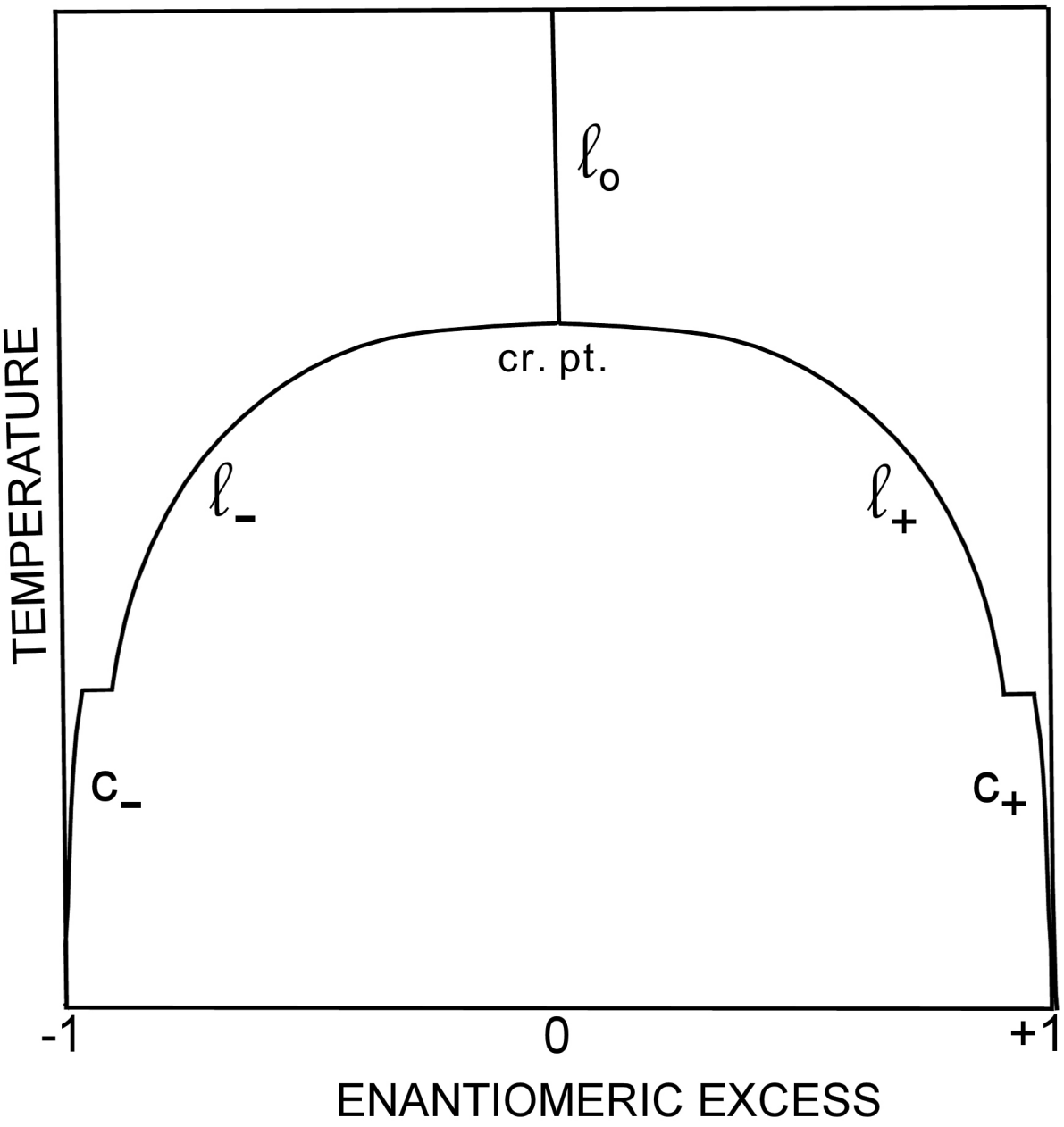
TEMPERATURE
ℓ_o
cr. pt.
ℓ_-
ℓ_+
c_-
c_+
-1
0
+1
ENANTIOMERIC EXCESS

Consolute Critical Point Pairs: Closed Coexistence Curves

- glycerol + guaiacol
  [B.C. McEwan, J. Chem. Soc. **123**, 2284-2288 (1923)]

- glycerol + m-toluidine
  [R.R. Parvatiker and B.C. McEwan, J. Chem. Soc. **125**, 1484-1492 (1924)]

- glycerol + ethylbenzylamine
  [R.R. Parvatiker and B.C. McEwan, J. Chem. Soc. **125**, 1484-1492 (1924)]

- water + nicotine
  [A.N. Campbell, E.M. Kartzmark, and W.E. Falconer, Can. J. Chem. **36**, 1475-1486 (1958)]

- water + 2-butoxyethanol
  [C.M. Ellis, J. Chem. Educ. **44**, 405-407 (1967)]

Basic Three-Dimensional Bravais Lattice Structure Consisting of *M* Cells

- Discrete cell occupancy variables ($1 \le i \le M$):

$$\begin{aligned} \nu_i &= -1 \quad \text{(left-handed chiral occupant L)} \\ &= 0 \quad \text{(empty cell)} \\ &= +1 \quad \text{(right-handed chiral occupant D)} \ . \end{aligned}$$

- Overall occupancy:

$$N_- = \sum_{i=1}^{M} \nu_i (\nu_i - 1)/2 \ ,$$

$$N_+ = \sum_{i=1}^{M} \nu_i (\nu_i + 1)/2 \ ,$$

$$N = N_- + N_+ = \sum_{i=1}^{M} (\nu_i)^2 \ .$$

- Potential energy invariant to overall particle mirror inversion:

$$\Phi(\nu_1, \nu_2 .... \nu_M) = \Phi(-\nu_1, -\nu_2 .... -\nu_M) \ .$$

View 16 (click to go back)

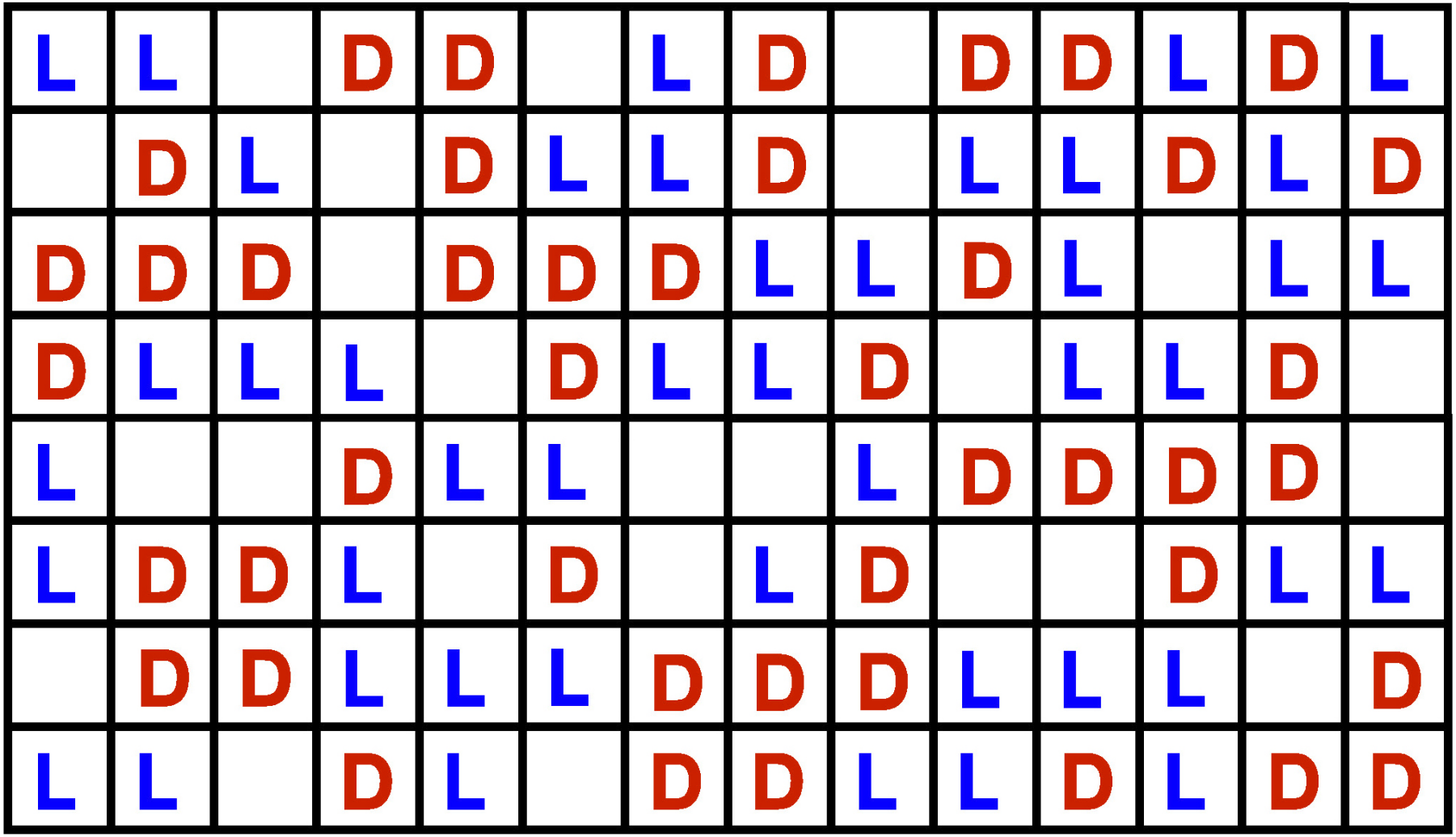

Lattice Model Potential Energy Assumption:

$$\Phi(\nu_1,\nu_2....\nu_M)=\sum_{i=2}^{M}\sum_{j=1}^{i-1}\left[\nu_i{}^2\nu_j{}^2\varphi_J(r_{ij})+\nu_i\nu_j\varphi_K(r_{ij})\right],$$

φ_J = chirality-independent pair interaction ,

φ_K = chirality-sensitive pair interaction ,

r_{ij} = scalar distance between cell centers .

Classical Canonical Partition Function for the Lattice Model:

$$Z(M,N,T)=\omega^N\sum_{\{\nu_i\}}^{(M,N)}\exp\left[-\Phi(\nu_1,\nu_2....\nu_M)/k_BT\right]$$

$$\equiv\exp\left[-F(M,N,T)/k_BT\right];$$

F = Helmholtz free energy, ω = cell volume.

Mean Field Approximation

- Basic assumption: Local particle distribution around any chosen occupied site is equal to the system's average distribution.

- Interaction simplifications ($J, K < 0$):

$$\sum_{i=2}^{M} \varphi_J(r_{1i}) \to J \quad , \qquad \sum_{i=2}^{M} \varphi_K(r_{1i}) \to K \quad .$$

- Simplified free energy expression:
$-F(M,N,T)/Nk_BT$

$$\approx \ln\omega + \left(\frac{M}{N}\right)\ln\left(\frac{M}{N}\right) - \left(\frac{M}{N}-1\right)\ln\left(\frac{M}{N}-1\right) + \ln 2 - \left(\frac{JN}{2Mk_BT}\right)$$

$$+ \frac{1}{2}\underbrace{\max}_{x}\left\{-(1+x)\ln(1+x) - (1-x)\ln(1-x) - \left(\frac{KN}{Mk_BT}\right)x^2\right\} \quad .$$

- Intensive variable $-1 \le x \le +1$ measures overall chirality:
$N_+ = (1+x)N/2$, $N_- = (1-x)N/2$.

Chiral Symmetry Breaking for $|J|<<|K|$

- Condition on intensive chirality variable x to minimize $F(N,M,T)$ expression:

$$\frac{1+x}{1-x} = \exp\left[-\left(\frac{2K\rho}{k_B T}\right)x\right] \quad ,$$

where $\rho = N/M$.

- If $k_B T > -K\rho$ ($K<0$) the only real solution is $x = 0$ (racemic state).
  If $k_B T < -K\rho$ there is a symmetric pair of non-zero solutions $\pm x(T,\rho)$.

- Chiral symmetry breaking critical point: $k_B T_{\pm} = -K\rho$.

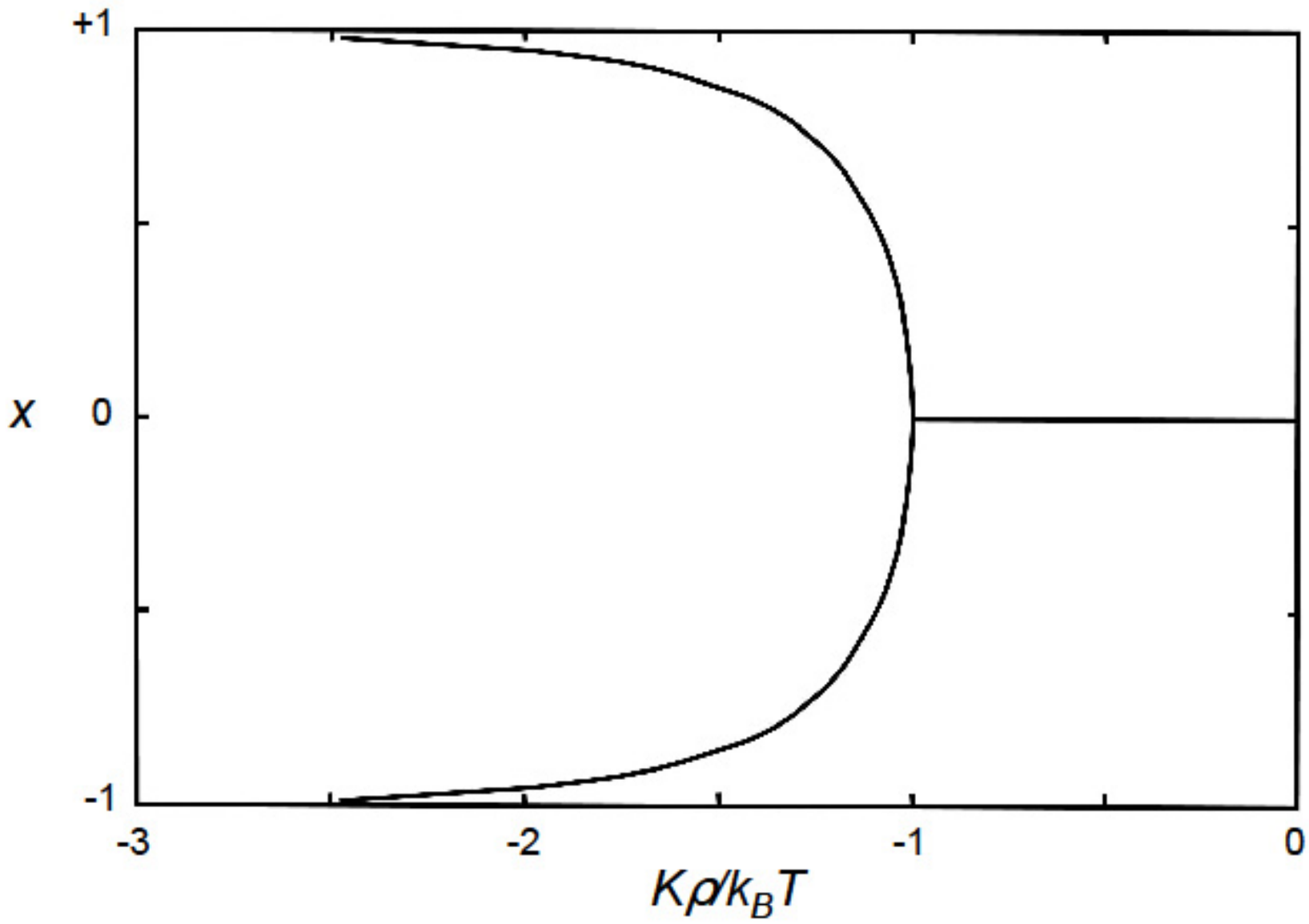
+1
X
0
-1
-3
-2
-1
0
$K\rho/k_BT$

Liquid-Vapor Transition

- Temporarily assume $|J| >> |K|$ so that the temperature range of liquid-vapor phase separation begins well above any $T_{\pm}$.

- Free energy for the racemic fluid system:

$$-F/k_BT \approx N\ln\omega + M\ln M - (M-N)\ln(M-N)$$
$$-N\ln\left(\frac{N}{2}\right) - \left(\frac{JN^2}{2Mk_BT}\right) \quad .$$

- Locating the critical point and the coexisting liquid-vapor densities requires the pressure formula:

$$p = -\left(\frac{\partial F}{\partial V}\right)_T \approx -\frac{1}{\omega}\left(\frac{\partial F}{\partial M}\right)_T \quad .$$

- Lattice model: $p\omega = -k_BT\ln(1-\rho) + J\rho^2/2$.

Liquid-Vapor Transition Densities Located by the Homogeneous System Pressure Formula

- The critical point and spinodal curves are located by the condition:

$$0 = \left(\frac{\partial p\omega}{\partial (1/\rho)} \right)_T = -\rho^2 \left(\frac{\partial p\omega}{\partial \rho} \right)_T = \left(\frac{\rho^2}{1-\rho} \right) \left[J\rho^2 - J\rho - k_B T \right] \ .$$

- Real solutions: $\rho = (1/2)[1 \pm (1 + 4k_B T / J)^{1/2}]$.

- Critical point: $k_B T_{lv} = -J/4$; $\rho_{lv} = 1/2$.

- Maxwell construction for equal liquid-vapor chemical potentials at coexistence ($T < T_{lv}$) implies:

$$\rho_l, \rho_v = (1/2)[1 \pm (3\eta)^{1/2}] + O(\eta) \ , \qquad \eta = 1 + 4k_B T / J \ .$$

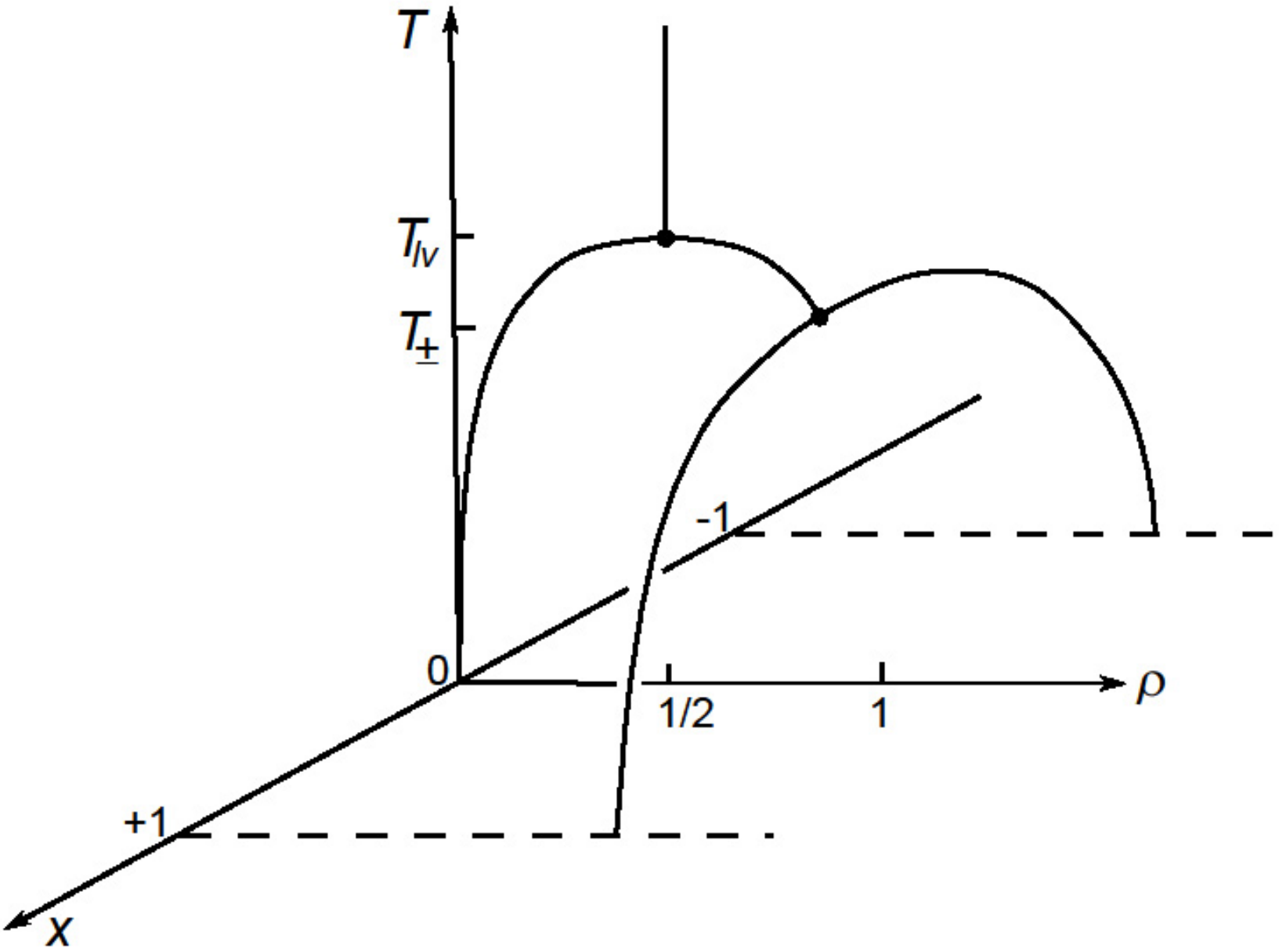
T
T_{lv}
$T_{\pm}$
-1
0
1/2
1
ρ
+1
x

Critical Point Confluence Condition

- Participation of liquid-vapor critical point requires $\rho = N/M = 1/2$.
- Requirement that $T_{lv} = T_{\pm}$ implies $J = 2K$.
- Therefore: $k_B T_{cfl} = |J|/4 = |K|/2$, and $\rho_{cfl} = 1/2$.
- As T declines through T_{cfl} , three fluid phases arise: Two chiral liquids, and a racemic vapor.
- Two distinct interfacial free energies appear for $T < T_{cfl}$:
  - (a) Contact interface between opposite chirality liquids;
  - (b) Chiral liquid-racemic vapor interface.

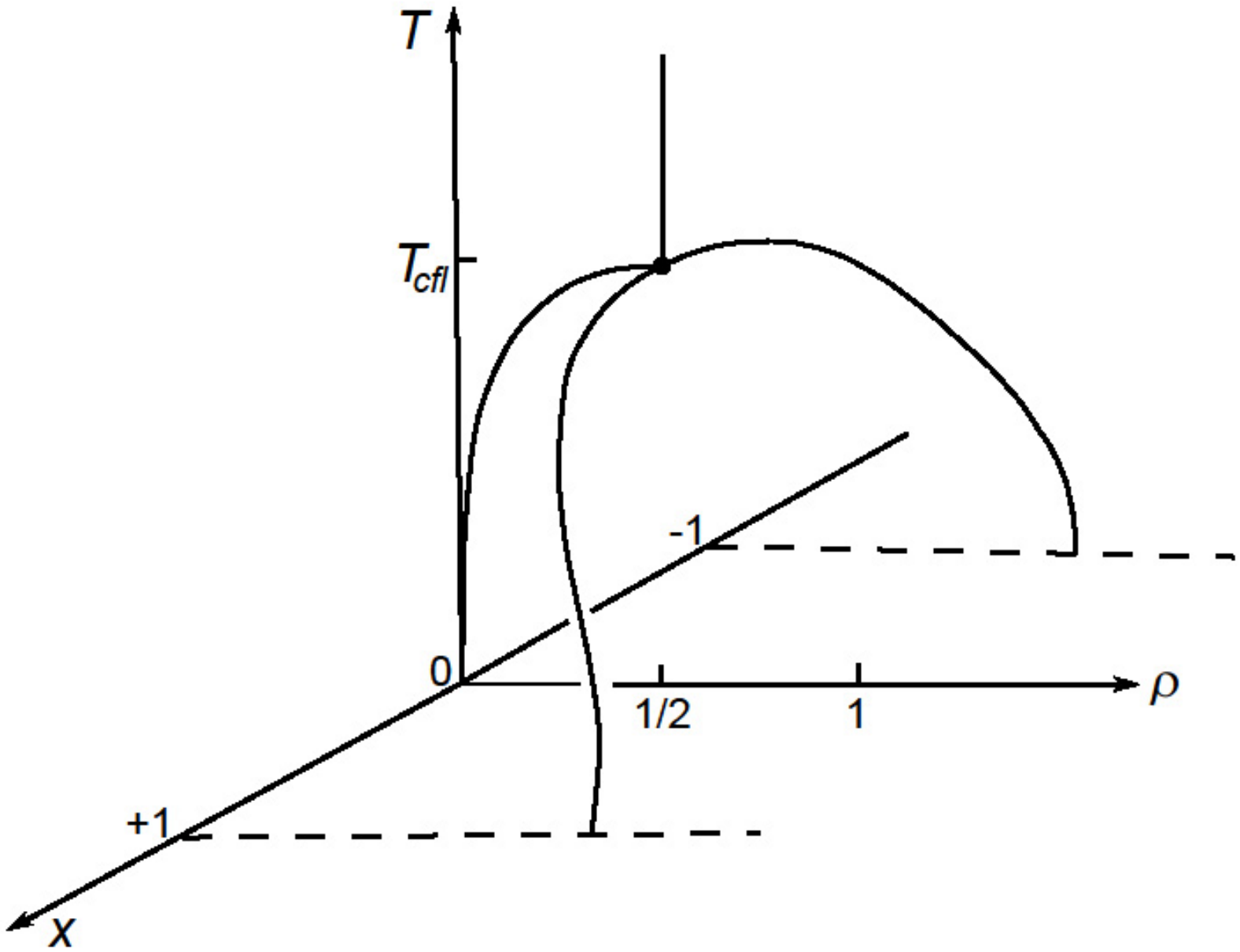
T
T_{cfl}
-1
0
1/2
1
ρ
+1
x

Critical Exponent Modification Due to Critical Point Confluence

- Define: $\Delta T = T_{cfl} - T > 0$, $\Delta\rho = \rho - 1/2$.

- Unlike the liquid-vapor critical point, the chiral-symmetry breaking critical point can occur over a variable density range:
$$k_B T_{\pm} = -K(1/2 + \Delta\rho) \quad .$$

- In the mean field approximation, the liquid branch in the liquid-vapor separation effect involves a leading-order density increase:
$$\Delta\rho \propto (\Delta T)^{1/2} \quad .$$

- The spontaneous chirality measure x at fixed T moves away from zero as a result of a density increment:
$$x \propto \pm(\Delta\rho)^{1/2} \quad .$$

- Therefore: $x(\Delta t) \propto \pm[(\Delta T)^{1/2}]^{1/2} = (\Delta T)^{1/4}$.
This constitutes reduction of a critical exponent by one-half.

Experimental and Theoretical Future Research Opportunities

(1) Synthesize more molecules possessing isotropic chiral liquid phases.

(2) Undertake molecular dynamics search for liquid-vapor critical points in tetramer continuum models.

(3) Use Monte Carlo simulations to determine interaction range effects for the lattice model family.

(4) Create renormalization group analyses for the lattice and continuum models to determine their precise critical confluence exponents.

(5) Measure interfacial tensions *vs.* temperature for chiral liquids.

(6) Determine the stable crystal structures for the tetramer model for different choices of potential energy parameters.